Metal-ligand cooperativity promotes reversible capture of dilute CO_2 as a Zn(II)-methylcarbonate

Christine A. Phipps, Dillon T. Hofsommer, Calian D. Zirilli, Bailee G. Duff, Mark S. Mashuta, Robert M. Buchanan, Craig A. Grapperhaus**

Department of Chemistry, University of Louisville, 2320 S. Brook St, Louisville, KY 40292

Corresponding Author

robert.buchanan@louisville.edu

craig.grapperhaus@louisville.edu

ABSTRACT: In this study, a series of thiosemicarbazonato- hydrazinatopyridine metal complexes were evaluated as to CO_2 capture agents. The complexes incorporate a non-coordinating, basic hydrazinatopyridine in close proximity to a Lewis acidic metal ion allowing for metal-ligand cooperativity. The coordination of various metal ions with (diacetyl-2-(4-methyl-thiosemicarbazone)-3-(2-hydrazinopyridine) (H_2L^1) yielded ML^1 (M = Ni(II), Pd(II)), $ML^1(CH_3OH)$ (M = Cu(II), Zn(II)), and $[ML^1(PPh_3)_2]BF_4$ (M = Co(III)) complexes. The $ML^1(CH_3OH)$ complexes reversibly capture CO_2 with equilibrium constants of 88 ± 9 and 6900 ± 180 for Cu(II) and Zn(II), respectively. Ligand effects were evaluated with Zn(II) through variation of the 4-methyl-thiosemicarbazone with 4-ethyl (H_2L^2), 4-phenethyl (H_2L^3), and 4-benzyl (H_2L^4). The equilibrium constant for CO_2 capture increased to 11,700 ± 300, 15,000 ± 400, and 35,000 ± 200 for $ZnL^2(MeOH)$, $ZnL^3(MeOH)$, and $ZnL^4(MeOH)$, respectively. Quantification of ligand basicity and metal ion Lewis acidity show that changes in CO_2 capture affinity are largely associated with ligand basicity upon substitution of Cu(II) with Zn(II), while variation of the thiosemicarbazone ligand enhances CO_2 affinity by tuning the metal ion Lewis acidity. Overall, the Zn(II) complexes effectively capture CO_2 from dilute sources with up to 90%, 86%, and 65% CO_2 capture efficiency from 400 ppm, 1000 ppm, and 2500 ppm CO_2 streams.

Introduction

The direct air capture (DAC) of carbon dioxide from air has been studied since the 1930s to prevent process equipment fouling[1] and to remove CO_2 from sealed vessels such as submarines[2] and spaceships.[3] More recently, CO_2 DAC has been under intense investigation as part of the strategy to mitigate the progression of climate change resulting from global fossil fuel based economies.[4] The DAC approach provides a means to concentrate and release CO_2 for utilization as a chemical feedstock for applications such as fuel production, agricultural usage, and the synthesis of other valuable products.[5] The current industrial standard for CO_2 DAC is a thermal cycle, where aqueous monoethanolamine is used as a nucleophile to capture CO_2 from a mixed gas stream and is released at elevated temperatures. This process operates at a 90% capture efficiency with flue gas but utilizes environmentally hazardous chemicals. Other small molecules capable of capturing and releasing CO_2 upon heating include N-heterocyclic olefins, which also catalyze the cycloaddition reaction of CO_2 with epoxides at higher pressures.[6] A promising alternative to aqueous amines are small molecule metal complexes that capture CO_2 by exploiting metal-ligand cooperativity (MLC). While there are many promising reports of MLC in large systems such as MOFs[7-9] or polymers,[10] this study will focus on discreet molecular compounds capable of CO_2 capture and release.

Metal-ligand cooperativity has been used in various catalysis applications such as C-C bond activation,[11-13] C-N bond activation,[14-16] cycloaddition/cyclization,[17-19] and hydrogenation.[20-22] There are four known classes of MLC: (1) the use of the metal or ligand as a Lewis base or (2) Lewis acid to cleave the substrate bond; (3) aromatic chelating ligands where dearomatization of the ligand allows for cooperation between the metal and ligand; and (4) use of redox non-innocent ligands that act as an electron reservoir during catalysis.[23] Many studies have focused on the use

of MLC to capture and activate CO_2 during its electrocatalytic reduction.[24-28] However, few studies have systematically evaluated modification of ligand structure to tune MLC in order to control CO_2 capture and release.[29]

We recently reported the CO_2 capture and electrochemical reduction based on the MLC properties of (diacetyl-2-(4-methyl-3-thiosemicarbazone)-3-(2-hydrazinatopyridine))zinc(II) (ZnL^1).[30] The ZnL^1 complex contains a unique, non-coordinating basic nitrogen on the hydrazinatopyridine moiety in close proximity to the Lewis acidic Zn(II) metal center. The basic nitrogen and Lewis acidic metal react cooperatively to reversibly capture CO_2 as a zinc-coordinated methylcarbonate complex. In this study, we explore a series of related complexes for reversible CO_2 capture from dilute sources to evaluate the effect of metal substitution and ligand variation, Figure 1, through measurement of ligand pK_a values and CO_2 capture equilibrium constants.

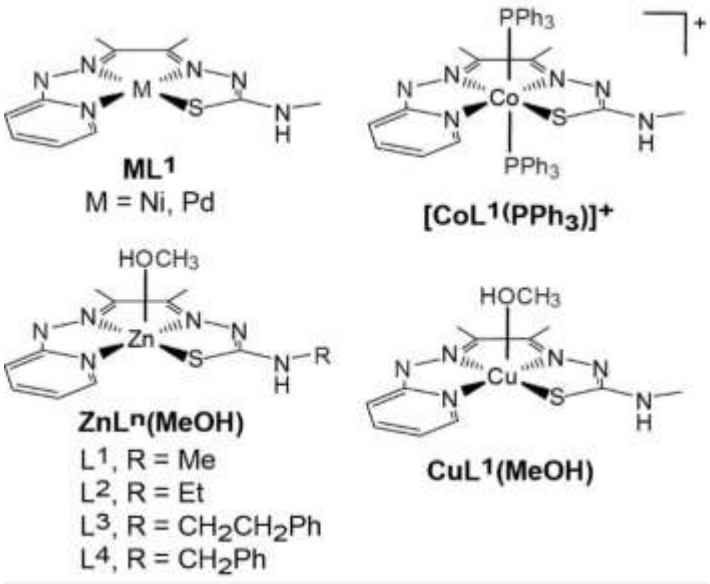

Figure 1. Thiosemicarbazonato-hydrazinatopyridine metal complexes in the current study.

Experimental

Materials and Methods

All solvents and materials were purchased as reagent grade from VWR or Sigma-Aldrich. H_2L^1 (diacetyl-2-(4-methyl-thiosemicarbazone)-3-(2-hydrazinopyridine)) was isolated in high yields from the procedure published by Cowley et al.[31] and the NiL^1, PdL^1, CuL^1(MeOH), and ZnL^1(MeOH) complexes were synthesized using the previously reported methods.[31-33] For the other ligands, the thiosemicarbazide precursors were synthesized as described previously for 4-benzyl-3-thiosemicarbazide.[34] All complexes and ligands in this study are stable in air and water and did not require protection from the atmosphere.

Diacetyl mono(2-pyridyl)hydrazone: The following procedure is a modification of the reported synthesis.[35] 24.14 g (0.2212 mol) of 2-hydrazinopyridine was dissolved in 100 mL of hot ethanol. 21.1 mL (0.242 mol) of 2,3-butanedione was then added and the mixture was refluxed for 30 minutes. The solution was then placed at -20 °C for one hour yielding a yellow precipitate. The solution was filtered to isolate 26.58 g (0.1500 mol) of an orange crystalline solid (67.8% yield). ^{1}H NMR (DMSO, d_6, 700 MHz) δ: 1.97 (3H, s), 2.35 (3H, s), 6.91 (1H, t, 6 Hz), 7.34 (1H, d, 8 Hz), 7.71 (1H, t, 8 Hz), 8.19 (1H, d, 4 Hz), 10.36 (1H, s). ^{13}C NMR (DMSO, d_6, 176 MHz) δ: 9.13, 24.13, 107.77, 117.30, 138.39, 142.96, 147.72, 156.35, 196.54. FT-IR (ATR): 3356 (vw), 3328 (w), 3241 (w), 1595 (m), 1574 (m), 1512 (s), 1489 (s), 1439 (m), 1419 (m), 1366 (w), 1323 (m), 1296 (m), 1268 (w), 1213 (s), 1194 (m), 1176 (m), 1139 (m), 1101 (m), 1074 (m), 1027 (w), 983 (w), 961 (w), 769 (m), 751 (m), 701 (w), 673 (w), 628 (m), 591 (m), 547 (m) cm^{-1}. Elemental analysis for $C_9H_{11}N_3O$ calc: C, 61.00; H, 6.26; N, 23.71. Found: C, 61.17; H, 5.96; N, 23.64.

(diacetyl-2-(4-ethyl-thiosemicarbazone)-3-(2-hydrazinopyridine)) H_2L^2: 321 mg (1.81 mmol) of diacetyl mono(2-pyridyl)hydrazone was dissolved in 60 mL of refluxing ethanol. Then 215 mg (1.80 mmol) 4-ethyl-3-thiosemicarbazide was added with 20 drops glacial acetic acid and the mixture was refluxed for two days. The round bottom was cooled to -20 °C for two hours. The resultant precipitate was filtered and washed with 20 mL of cold diethyl ether. 422 mg (1.52 mmol) of an off-white powder was isolated, 83.8%. ^{1}H NMR (DMSO, d_6, 700 MHz) δ: 1.15 (t, 3H, 7 Hz), 2.21 (d, 6 H, 2 Hz), 3.60 (t, 2H, 10 Hz), 6.84 (t, 1H, 6 Hz), 7.26 (d, 1H, 8 Hz), 7.67 (t, 1H, 8 Hz), 8.16 (d, 1H, 3 Hz), 8.33 (t, 1H, 6 Hz), 9.90 (s, 1H), 10.06 (s, 1H) ppm. ^{13}C NMR (DMSO, d_6, 176 MHz) δ: 11.43, 14.48, 107.07, 115.89, 138.09, 144.10, 147.63, 148.79, 157.09, 177.32 ppm. FT-IR (ATR): 3353 (w), 3334 (w), 3249 (br), 2961 (w), 2360 (w), 1594 (m), 1575 (m), 1509 (s), 1481 (s), 1441 (s), 1380 (m), 1315 (m), 1294 (m), 1270 (m), 1218 (m), 1171 (s), 1133 (m), 1101 (s), 1083 (m), 823 (m), 856 (m), 830 (w), 771 (s), 738 (w), 678 (m), 629 (w), 589 (w), 551 (w) cm^{-1}. Elemental analysis for $C_{12}H_{18}N_6S$ calc: C, 51.78; H, 6.52; N, 30.19. Found: C, 51.66; H, 6.47; N, 29.90.

(diacetyl-2-(4-phenethyl-thiosemicarbazone)-3-(2-hydrazinopyridine)) H_2L^3: 591 mg (3.03 mmol) 4-phenethyl-thiosemicarbazide and 537 mg (3.03 mmol) of diacetyl mono(2-pyridyl)hydrazone were dissolved in 40 mL of refluxing ethanol. 15 drops of glacial acetic acid were added to the solution, and the mixture was refluxed for two days. The solution was then cooled to -20 °C until a white precipitate formed. The precipitate was filtered and rinsed with cold diethyl ether to obtain 808 mg (2.28 mmol) off-white solid (75.2% yield). ^{1}H NMR (DMSO, d_6, 700 MHz) δ: 2.15 (s, 3H), 2.22 (s, 3H), 2.91 (t, 2H, 7 Hz), 3.80 (q, 2H, 5 Hz), 6.84 (d, 1H, 13 Hz), 7.28 (m, 5H), 7.67 (t, 1H, 8 Hz), 8.16 (d, 1H, 6 Hz), 8.30 (t, 1H, 6 Hz), 9.91 (s, 1H), 10.22 (s, 1H) ppm. ^{13}C NMR (DMSO, d_6, 176 MHz) δ: 10.84, 11.50, 34.65, 45.17, 107.09, 115.93, 125.24

128.49, 128.63, 138.09, 139.23, 143.93, 147.63, 148.95, 157.08, 177.58 ppm. FT-IR (ATR): 3357 (vw), 3333 (vw), 3215 (br), 2863 (vw), 2360 (w), 1595 (m), 1573 (m), 1495 (s), 1467 (s), 1439 (s), 1391 (w), 1298 (m), 1221 (m), 1173 (m), 1141 (m), 1075 (m), 1050 (w), 983 (w), 920 (w), 768 (m), 748 (m), 737 (m), 700 (w), 677 (w), 590 (m) cm^{-1}. Elemental analysis for $C_{18}H_{22}N_6S$ calc: C, 60.99; H, 6.26; N, 23.71. Found: C, 60.58; H, 5.94; N, 23.63.

(diacetyl-2-(4-benzyl-thiosemicarbazone)-3-(2-hydrazinopyridine)) H_2L^4: 500 mg (2.76 mmol) of 4-benzyl-thiosemicarbazide and 507 mg (2.86 mmol) of diacetyl mono(2-pyridyl)hydrazone were dissolved in refluxing ethanol with 20 drops of glacial acetic acid. The solution was then refluxed for two days and placed to cool in the freezer at -20 C overnight. The solution was then filtered, rinsed with diethyl ether, and 715 mg (2.10 mmol) of a yellow powder was isolated (73.4% yield). ^{1}H NMR (DMSO, *d*$_6$, 700 MHz): 2.21 (s, 3H), 2.25 (s, 3H), 4.86 (d, 2H, 6 Hz), 6.64 (t, 1H, 6 Hz), 7.25 (m, 2H, 5 Hz), 7.34 (m, 4H, 5 Hz), 7.67 (t, 1H, 7 Hz), 8.16 (s, 1H), 8.85 (s, 1H), 9.90 (s, 1H), 10.27 (s, 1H). ^{13}C NMR (DMSO, *d*$_6$, 176 MHz) δ: 10.91, 11.55, 46.81, 107.10, 115.92, 126.73, 127.17, 128.19, 138.10, 139.35, 144.06, 147.62, 149.29, 157.06, 178.25. FT-IR (ATR): 3556 (w), 3328 (w), 3241 (br), 1595 (m), 1574 (m), 1516 (m), 1489 (s), 1439 (m), 1419 (m), 1366 (w), 1296 (m), 1268 (m), 1194 (m), 1139 (m), 1074 (m), 982 (w), 769 (m), 701 (m), 628 (m), 591 (m), 547 (w). Elemental analysis for $C_{17}H_{20}N_6S$ calc: C, 59.98; H, 5.92; N, 24.69. Found: C, 59.50; H, 5.45; N, 24.43.

(diacetyl-2-(4-methyl-thiosemicarbazonato)-3-(2-hydrazinatopyridine))-bis(triphenylphosphino)cobalt(III) tetrafluoroborate, $[CoL^1(PPh_3)_2]BF_4$: H_2L^1 (275 mg, 1.04 mmol) and hexaaquocobalt (II) tetrafluoroborate (360 mg, 1.05 mmol) were suspended in 10 mL of ethanol. To the brown slurry was added triethylamine (0.3 mL) and triphenylphosphine (554 mg, 2.11 mmol). The brown suspension was heated to reflux for 1 hour, cooled to room

temperature, and placed in a freezer. The resultant dark solid was filtered and washed with 5 mL of cold ethanol and 20 mL of diethyl ether and dried under vacuum to obtain 550 mg (0.650 mmol) brown solid (62.5% yield). Single crystals suitable for X-ray diffraction were obtained by vapor diffusion of a saturated MeCN solution with diethyl ether. ^{1}H NMR (DMSO, *d*$_6$, 700 MHz) δ: 2.04-2.28 (9 H, br), 6.01 (br, 1H), 6.36 (br, 1H), 6.99-7.90 (38 H, br) ppm. ^{19}F NMR (DMSO, *d*$_6$, 376 MHz) δ: -148.40 ppm. ^{31}P NMR (DMSO, *d*$_6$, 162 MHz) δ: 15.87 ppm. FT-IR (ATR): 1608 (w), 1509 (s), 1481 (m), 1455 (w), 1432 (s), 1399 (s), 1307 (vs), 1221 (s), 1136 (w), 1049 (vs), 988 (s), 841 (w), 777 (w), 751 (s), 693 (vs), 646 (w) cm^{-1}. UV-Vis (MeCN, 10^{-4} M): 261 nm (52,400 M^{-1}cm^{-1}), 556 nm (6,610 M^{-1} cm^{-1}). Anal calc for $C_{47}H_{44}BCoF_4N_6P_2S$: C 60.53, H 4.76, N 9.01. Found C 60.29, H 5.10, N 8.94.

(diacetyl-2-(4-ethyl-3-thiosemicarbazato)-3-(2-hydrazinatopyridine))zinc(II), ZnL^2: In a round bottom flask with 50 mL of refluxing ethanol, 212 mg (0.762 mmol) of H_2L^2 and 65 mg (1.5 mmol) of LiOH were added and the solution refluxed for 10 minutes. Then, 168 mg (0.765 mmol) of $Zn(OAc)_2$ was added and the solution immediately turned orange. The solution was refluxed for an additional 4 hours and then chilled in the freezer for one hour. 185 mg (0.541 mmol) of a bright orange powder was isolated (71.0% yield). ^{1}H NMR (DMSO, *d*$_6$, 700 MHz): 1.11 (t, 3H, 7 Hz) 2.12 (s, 3H), 2.15 (s, 3H), 6.24 (t, 1H, 6 Hz), 6.55 (d, 1H, 9 Hz), 6.99 (s, 1H), 7.26 (t, 1H, 8 Hz), 7.44 (d, 1H, 5 Hz). The methylene protons at 3.25 ppm are not observed in the ^{1}H but are observed in the COSY (Fig. S14). ^{13}C NMR (DMSO, *d*$_6$, 176 MHz) δ: 12.14, 13.56, 14.71, 37.13, 109.79, 116.24, 135.84, 137.76, 145.34, 147.03, 164.50, 171.93, 174.78. FT-IR (ATR): 3341 (w), 2695 (w), 1602 (m), 1542 (m), 1535 (m), 1482 (m), 1419 (s), 1372 (m), 1335 (m), 1297 (s), 1253 (m), 1214 (s), 1153 (m), 1082 (m), 991 (m), 825 (m), 772 (m), 643 (m) cm^{-1}. Elemental analysis for $C_{14}H_{21}N_6SOZn$ calc: C, 40.37; H, 4.43; N, 21.73. Found: C, 39.33; H, 4.51; N, 21.66

(diacetyl-2-(4-phenethyl-3-thiosemicarbazato)-3-(2-hydrazinatopyridine))zinc(II), ZnL^3: In a round bottom flask with 30 mL of refluxing ethanol, 178 mg (0.502 mmol) of H_2L^3 and 45 mg (1.1 mmol) of LiOH were added. After 10 minutes, 116 mg (0.528 mmol) of $Zn(OAc)_2$ was added resulting in an immediate color change to orange. After refluxing for an additional 4 hours, the solution was cooled in an ice bath and filtered. 193 mg (0.462 mmol) of a bright orange powder was isolated (91.4% yield). Single crystals were isolated by slow evaporation of a saturated CO_2 sparged methanol solution. ^{1}H NMR (DMSO, d_6, 700 MHz) δ: 2.13 (s, 3H), 2.19 (s, 3H), 2.87 (d, 2H, Hz), 3.51 (d, 2H, Hz), 6.25 (s, 1H), 6.56 (d, 1H, 9 Hz), 7.11 (s, 1H), 7.19 (t, 1H, 7 Hz), 7.23-7.29 (m, 5H), 7.46 (s, 1H) ppm. ^{13}C NMR (DMSO, d_6, 176 MHz) δ: 12.14, 13.63, 34.99, 44.32, 109.84, 116.33, 125.98, 128.35, 128.63, 135.68, 139.98, 145.36, 147.48, 164.56, 176.12, 179.86 ppm. FT-IR (ATR): 3335 (br), 2917 (w), 2858 (w), 2359 (w), 1602 (m), 1519 (m), 1476 (m), 1420 (m), 1336 (m), 1293 (m), 1229 (m), 1213 (m), 1194 (m), 1148 (m), 1093 (m), 1048 (m), 991 (m), 879 (w), 820 (m), 763 (m), 750 (m), 701 (m), 646 (m), 597 (w), 559 (w) cm^{-1}. Elemental analysis for $C_{18}H_{20}N_6SZn$ calc: C, 51.74; H, 4.82; N, 20.11. Found: C, 51.53; H, 5.00; N, 20.17.

(diacetyl-2-(4-benzyl-3-thiosemicarbazato)-3-(2-hydrazinatopyridine))zinc(II), ZnL^4: In a round bottom flask with 40 mL of refluxing ethanol, 170 mg (0.499 mmol) of H_2L^4 and 42 mg (1.0 mmol) of LiOH were added. After 10 minutes, 107 mg (0.487 mmol) of $Zn(OAc)_2$ resulting in an immediate color change to orange. After refluxing for an additional 4 hours, the solution was cooled to room temperature and placed in a freezer overnight. Filtration yielded 104 mg (0.258 mmol) of a bright orange powder (52.9% yield). Single crystals were grown by slow evaporation in methanol. ^{1}H NMR (DMSO, d_6, 700 MHz) δ: 2.10 (s, 3H), 2.11 (s, 3H), 4.50 (d, 2H, 5 Hz), 6.25 (s, 1H), 6.54 (d, 1H, 9 Hz), 7.19 (t, 1H, 4 Hz), 7.29 (m, 3H, 4 Hz), 7.33 (d, 2H, 7 Hz), 7.45 (s, 1H), 7.57 (s, 1H) ppm. ^{13}C NMR (DMSO, d_6, 176 MHz) δ: 12.06, 13.55, 35.01, 44.29, 109.70, 109.85,

116.26, 116.36, 125.85, 126.06, 128.50, 128.68, 135.63, 137.63, 137.82, 139.95, 145.24, 145.42, 164.57 ppm. FT-IR (ATR): 3706 (s), 3680 (s), 3335 (w), 2973 (br), 2865 (s), 2075 (w), 2053 (w), 1602 (w), 1510 (w), 1455 (m), 1346 (s), 1322 (m), 1057 (s), 1014 (s), 882 (w), 818 (m), 765 (m), 732 (m), 646 (m), 603 (w) cm^{-1}. Elemental analysis for $C_{18}H_{22}N_6SOZn$ calc: C, 49.60; H, 5.09; N, 19.28. Found: C, 50.08; H, 5.45; N, 18.71.

Physical Methods

Elemental analysis was performed by Micro-Analysis Inc. (Wilmington, DE, USA) using TCD and combustion. NMR data was collected on Varian Inova 400 MHz and 700 MHz NMR spectrometers with deuterated DMSO purchased from Cambridge Isotopes. Infrared spectra were recorded on a ThermoFisher Nicolet iS20 FT-IR with an ATR attachment (0.25 cm^{-1} resolution) for solid samples or with a Specac CaF_2 IR cell for solution samples.

pH measurements

All pH titrations used a Horiba Scientific LAQUA ion meter F-72G pH probe filled with sat. KCl in methanol. Prior to use each day, the probe was calibrated with Horiba Scientific calibration pH standards at pH 2.00 (act. pH was 1.68, model 100-2), 4.00 (act. pH was 4.01, model 100-4), 7.00 (act. pH was 7.00, model 100-7U), and 10.00 (act. pH was 10.01, model 100-10U). In a typical experiment, 10 mg of complex was added to 20 mL of methanol, which had been sparged with argon for at least 30 minutes prior to use. During the experiment, the solution was constantly stirring and sparging with argon to prevent carbon dioxide contamination (methylcarbonic acid formation). The solution was stirred until the pH reading stabilized. For compounds that were relatively acidic, titration from the neutral species to the protonated species was performed using HBF_4 as titrant. A stock solution of HBF_4 was standardized each day using sodium carbonate and

phenolphthalein as an indicator. For more basic compounds ZnL^{1-4}(MeOH), the species was first protonated using an excess of the previously described standardized HBF_4 solution then titrated with KOH. KOH was standardized with KHP and phenolphthalein.

Crystallographic Studies

$[CoL^1(PPh_3)_2]BF_4$: The CrysAlisPro[36] CCD software package was used to acquire a total of 517 ten second frame ω-scan exposures of data for a purple prism crystal at 102 K to a 2θ max = 60.92° using monochromated MoKα radiation (0.71073 Å) from a sealed tube. Frame data were processed using CrysAlisPro RED to determine final unit cell parameters: a = 12.7669(4) Å, b = 15.2243(4) Å, c = 24.4256(7) Å, α= 90°, β = 102.715(3)°, γ = 90°, V = 4631.1(2) $Å^3$, D_{calc} = 1.421 mg/m^3, Z = 4 to produce raw hkl data that were then corrected for absorption (transmission min./max. = 0.886 /1.000; μ = 0.547 mm^{-1}) using SCALE3 ABSPACK.[37] The structure was solved using Patterson methods in the space group $P2_1/c$ using SHELXS[38] and refined by least squares methods on F^2 using SHELXL.[38] Non-hydrogen atoms were refined with anisotropic atomic displacement parameters. The BF_4 counter ion was modeled using a spinning top disorder with full one occupancy B1 and F1 atom. 0.70 occupancy F2a, F3a, F4a and 0.15 occupancy F2b, F3b, F4b, F2c, F3c, and F4c atoms were used to complete the disorder model applying 15 geometric restraints. The nitrogen H was located by difference maps and refined isotropically. Methyl and phenyl hydrogen atoms were placed in their geometrically generated positions and refined as a riding model and these atoms were respectively assigned U(H) = 1.5 and 1.2 x Ueq. For all 14,055 unique reflections (R(int) 0.034) the final anisotropic full matrix least-squares refinement on F^2 for 604 variables converged at R_1 = 0.059 and wR_2 = 0.124 with a GOF of 1.02.

ZnL^3(MeOH): An orange plate 0.35 x 0.10 x 0.02 mm^3 crystal grown from a solution of methanol in a round bottom flask was mounted on a CryoLoop for collection of X-ray data on an Agilent Technologies/Oxford Diffraction Gemini CCD diffractometer. The CrysAlisPro[36] CCD software package (v 1.171.40.67a) was used to acquire a total of 956 twenty-three second frame ω-scan exposures of data at 102 K to a 2θ max = 57.40° using monochromated MoKα radiation (0.71073 Å) from a sealed tube. Frame data were processed using CrysAlisPro[36] RED to determine final unit cell parameters: a = 7.4714(5) Å, b = 11.8168(7) Å, c = 11.8709(7) Å, α = 95.509(5)°, β = 98.512(5)°, γ = 106.554(5)°, V = 982.93(11) $Å^3$, D_{calc} = 1.520 mg/m^3, Z = 2 to produce raw hkl data that were then corrected for absorption (transmission min./max. = 0.736/1.00; μ = 1.379 mm^{-1}) using SCALE3 ABSPACK.[37] The structure was solved by Direct methods in the triclinic space group P-1 using SHELXS[38] and refined by least squares methods on F^2 using SHELXL.[38] Non-hydrogen atoms were refined with anisotropic atomic displacement parameters. Hydrogen atoms were placed in their geometrically generated positions and refined as a riding model and these atoms were assigned U(H) = 1.5 x Ueq for methyl H's and 1.2 x Ueq for all other H's. For all 5057 unique reflections (R(int) 0.100) the final anisotropic full matrix least-squares refinement on F^2 for 312 variables converged at R^1 = 0.062 and wR^2 = 0.109 with a GOF of 1.04.

ZnL^4(MeOH): Crystals of ZnL^4(MeOH) suitable for x-ray analysis were grown by slow evaporation of a CO_2 saturated methanol solution. X-ray structural analysis for ZnL^4(MeOH) was performed on a 0.35 x 0.15 x 0.04 mm^3 orange plate using an identical data acquisition strategy described above for ZnL^3(MeOH) at 102 K to a $2\theta_{max}$ = 55.02°. ZnL^4(MeOH) crystallizes in the triclinic space group P1 bar with unit cell parameters: a = 7.5571(4) Å, b = 8.4581(4) Å, c = 15.4435(9) Å, α = 75.871(5)°, β = 76.936(5)°, γ = 86.110(4)°, V = 932.41(9) $Å^3$, Z = 2 and D_{calc} = 1.552 Mg/m^3· 4267 raw independent data from 501 fifty second frames were corrected for

absorption (transmission min./max. = 0.921 / 1.000; μ = 1.451 mm^{-1}) using SCALE3 ABSPACK.[37] The structure was solved by Patterson methods using SHELXTL. All non-hydrogen atoms were refined with anisotropic atomic displacement parameters. NH, OH, phenyl and methylene hydrogen atoms were located by difference maps and refined isotropically**.** Methyl hydrogen atoms were placed in their geometrically generated positions and refined as a riding model and these atoms were assigned U(H) = 1.5 x Ueq. For all 4,267 unique reflections (R(int) 0.058) the final anisotropic full matrix least-squares refinement on F^2 for 179 variables converged at R1 = 0.067 and wR2 = 0.089 with a GOF of 1.05.

Results and Discussion

Synthesis and Characterization

A series of metal complexes of the tetradentate ligand diacetyl-2-(4-methyl-3-thiosemicarbazone)-3-(2-hydrazinopyridine) (H_2L_1), Figure 1, were synthesized and characterized to evaluate the effect of metal variation on CO_2 capture. The complexes NiL^1, PdL^1, CuL^1(MeOH), ZnL^1(MeOH) were prepared as previously reported in the literature.[31-33] The computationally optimized structures of the Ni(II) and Pd(II) derivatives are square planar as expected for four-coordinate d^8 metal complexes with sharp NMR signals.[33] The Cu(II) and Zn(II) are square pyramidal with methanol solvent coordinated in the apical position. The Co(III) derivative, $[CoL^1(PPh_3)_2]BF_4$, was synthesized from H_2L^1, cobalt(II) tetrafluroborate, and triphenylphosphine upon reflux in solution under aerobic conditions. X-ray quality crystals of $[CoL^1(PPh_3)_2]BF_4$ were isolated by vapor diffusion of a concentrated acetonitrile solution with diethyl ether. The Co(III) sits in a pseudo-octahedral environment with trans PPh_3 donors and the N_3S donors of L_1^{2-} occupying the equatorial plane (Fig. S1).

To evaluate the effect of ligand modification on CO_2 capture, a series of ligands with variation of the thiosemicarbazone pendent amine and their Zn(II) complexes were prepared, Figure 1. By variation of the thiosemicarbazide reagent in the ligand synthesis, the methyl substituent on the pendent amine of H_2L^1 was replaced with ethyl (H_2L^2), phenethyl (H_2L^3), and benzyl (H_2L^4) amine. The corresponding Zn(II) complexes were prepared by refluxing a solution of the ligand with one equivalent of zinc(II) acetate and two equivalents of lithium hydroxide. All isolated zinc compounds are orange, air-stable compounds that were characterized by ^1H and ^{13}C NMR and FT-IR spectroscopies. For example, the ^1H NMR spectrum of H_2L^2 displays pyridyl resonances at 6.84, 7.26, 7.67, and 8.16 ppm that are shifted upfield to 6.24, 6.55, 7.26, and 7.44 ppm in ZnL^2(MeOH) (Fig. S13). Additionally, the IR spectrum of H_2L^2 displays a thioamide bend at 678 cm^{-1}, C=N thioamide stretching modes at 1509 and 1594 cm^{-1}, and an NH stretch at 3353 cm^{-1} that shift to 643 cm^{-1}, 1535 cm^{-1}, and 3341 cm^{-1} in ZnL^2(MeOH). Similar trends are observed in the spectra of $H_2L^{3,4}$ and their Zn(II) complexes, $ZnL^{3,4}$. X-ray quality crystals of ZnL^3(MeOH) and ZnL^4(MeOH) were grown from slow evaporation in methanol. In each complex, the Zn(II) ion sits in a distorted square pyramidal environment, Figure 2, similar to ZnL^1(MeOH).[30] A comparison of metric parameters is provided in Table S2.

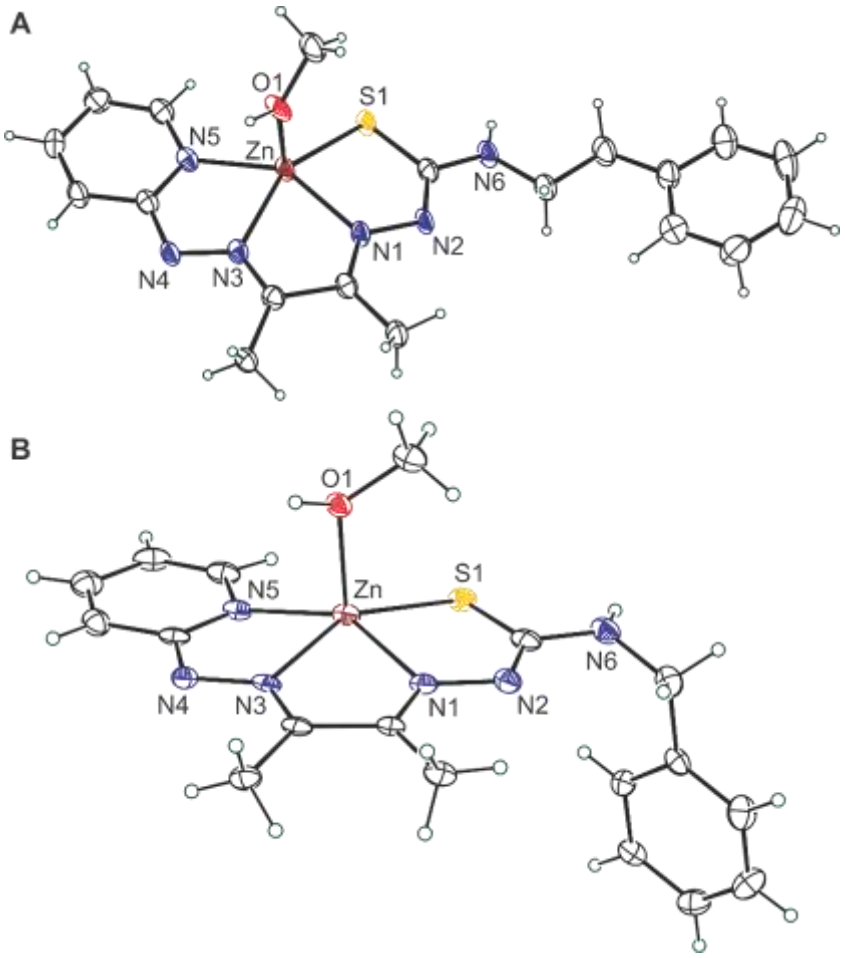

Figure 2. ORTEP representations of (A) ZnL^3(MeOH) and (B) ZnL^4(MeOH).

An overview of the electronic spectra of the ML^1 complexes and ML^n(MeOH) derivatives in methanol is provided in Table 1. The spectra of the complexes can be divided into two groups based on the number of observed charge transfer transitions associated with the 2-hydrazinatopyridine functional group in the region from 400 – 500 nm. For $[CoL^1(PPh_3)_2]^+$, NiL^1, PdL^1, a single band is observed in the 400 – 500 nm region associated with charge transfer between the metal ion and hydrazinatopyridine moiety of the $[L^1]^{2-}$ ligand (Fig. S24 – S26). The band shifts to higher energy for the six-coordinate Co(III) complex relative to the square planar Ni(II) and Pd(II) complexes. For CuL^1(MeOH) and ZnL^{1-4}(MeOH), the observed spectra include a lower

energy hydrazinatopyridine band associated with the neutral complex, $ML^n(MeOH)$, and a higher energy charge transfer band for its protonated derivative $[M(HL^n)(MeOH)]^+$. A representative spectrum of a 0.1 mM solution of $ZnL^2(MeOH)$ in methanol is shown in Figure 3. Spectra for other complexes are provided in Figures S20 – S23. The ratio of the two bands varies as a function of complex concentration as expected for acid-base equilibria. Spectra of the neutral complexes $ML^n(MeOH)$ were obtained through the addition of KOH to fully deprotonate the ligand. Similarly, the spectra for the $[M(HL^n)(MeOH)]^+$ complexes were obtained by the addition of collidinium hexafluorophosphate.

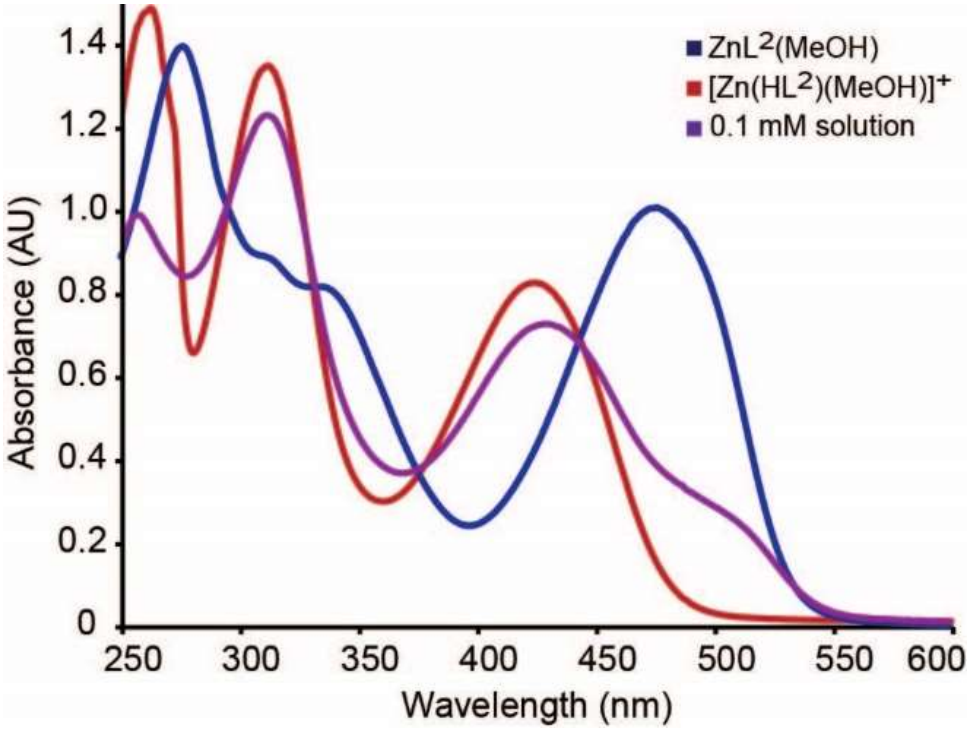

Figure 3. UV-vis spectra of 0.10 mM $ZnL^2(MeOH)$ with KOH added to shift equilibrium to $ZnL^2(MeOH)$ (blue), with collidinium hexafluorophosphate added to shift equilibrium to $[Zn(HL^2)(MeOH)]^+$ (red), and as prepared as a mixture of protonation states (purple).

Table 1. Comparison of ML^1 and $ZnL^n(MeOH)$ complexes in methanol.

Complex	**Color**	**UV-vis** λ_{max} **(ε** M^{-1} cm^{-1}**)**	**pK_a** $[M(HL^n)]^+$
$[CoL^1(PPh_3)_2]BF_4$	purple	568 (4150)	8.22 ± 0.15
NiL^1	green	700 (1760)	6.18 ± 0.05
PdL^1	blue	632 (5040)	5.23 ± 0.11
$CuL^1(MeOH)^a$	purple	515 (8660)	8.20 ± 0.08
$[Cu(HL^1)(MeOH)]^{+b}$	orange	471 (5100)	
$ZnL^1(MeOH)^a$	orange	478 (8570)	10.88 ± 0.09
$[Zn(HL^1)(MeOH)]^{+b}$	yellow	422 (3520)	
$ZnL^2(MeOH)^a$	orange	476 (5840)	10.99 ± 0.10
$[Zn(HL^2)(MeOH)]^{+b}$	yellow	424 (4400)	
$ZnL^3(MeOH)^a$	orange	476 (6340)	10.93 ± 0.05
$[Zn(HL^3)(MeOH)]^{+b}$	yellow	423 (4960)	
$ZnL^4(MeOH)^a$	orange	473 (4630)	10.29 ± 0.10
$[Zn(HL^4)(MeOH)]^{+b}$	yellow	421 (3250)	

[a]Samples prepared by addition of KOH to a solution of $ML^n(MeOH)$ in methanol under Ar.
[b]Samples prepared by addition of collidinium hexafluorophosphate to a solution of $ML^n(MeOH)$ in methanol under Ar.

To quantify the basicity of the non-coordinating, hydrazinatopyridine nitrogen as a function of metal and ligand variation, a series of titrations was conducted to determine the pK_a of the protonated $[M(HL^n)]^+$ and $[M(HL^n)(MeOH)]^+$ complexes. All titrations were conducted in methanol under a continuous argon purge to prevent reactivity with dissolved CO_2. As previously reported for $ZnL^1(MeOH)$, the non-coordinated, hydrazinatopyridine nitrogen is the site of protonation.[30] The NiL^1 and PdL^1 complexes were successfully titrated with HBF_4 with a color

change which accompanied the transition from the neutral to the protic species. For the remaining complexes, the pK_a was determined by back titration of the protonated complex due to the increased basicity of the hydrazinatopyridine nitrogen. All pK_a values are tabulated in Table 1. The square planar NiL^1 and PdL^1 complexes have the least basic hydrazinatopyridine nitrogen with associated pK_a values of 6.18 and 5.23, respectively. The complexes with coordinated methanol, CuL^1(MeOH) and ZnL^{1-4}(MeOH), are significantly more basic with observed pK_a values of 8.20 and 10.29 – 10.99, respectively. The ZnL^{1-4}(MeOH) complexes are more than 2 orders of magnitude more basic than CuL^1(MeOH) due to the greater Lewis acidity of Cu(II). For the series of Zn(II) complexes, ZnL^4(MeOH) is less basic than ZnL^{1-3}(MeOH), which have similar basicities.

Reversible CO_2 Capture

The various metal derivatives of H_2L^1 and Zn(II) derivatives of H_2L^{2-4} (Fig. 1) were evaluated to determine their ability to capture CO_2. Methanol solutions of each complex were sparged with CO_2 (1 atm) with monitoring by UV-visible spectroscopy. The square planar NiL^1 and PdL^1 and six-coordinate $[Co(L^1)(PPh_3)_2]^+$ complexes showed no spectral changes indicating these complexes have no affinity for CO_2. Solutions of the $Zn(L^{1-4})$(MeOH) complexes, on the other hand, uniformly displayed a rapid color change from orange to yellow upon the introduction of CO_2. The color change is associated with a change in the protonation state of the hydrazinatopyridine chromophore. Sparging of the solutions with Ar changed the yellow solution back to orange as the captured CO_2 was displaced indicating a reversible process, as shown in Figure S27. Similarly, the introduction of CO_2 into purple solutions of CuL^1(MeOH) resulted in a color change to orange, which can be reversed upon sparging with Ar.

Metal−ligand cooperativity facilitates the CO_2 capture as a metal-bound methylcarbonate, Figure 4. The non-coordinated, hydrazinatopyridine nitrogen serves as an intramolecular, Brønsted-Lowry base that is protonated in the CO_2 capture complex. The metal ion serves as a Lewis acid to stabilize the methylcarbonate anion. X-ray crystallographic studies on yellow single crystals grown from $ZnL^1(MeOH)$ under a CO_2 atmosphere confirm the identity of the CO_2 captured product as $Zn(HL^1)(O_2COMe)$.[30] Repeated attempts to obtain single crystals of the Cu(II) derivative and the $Zn(HL^{2-4})(O_2COMe)$ analogues were unsuccessful. Product identity was confirmed by FT-IR and ^1H NMR spectroscopy. The addition of CO_2 to $Zn(L^n)(MeOH)$ in CD_3OD:CH_3OH (25:75) shifts all ^1H NMR resonances downfield as expected for the $Zn(HL^n)(O_2COMe)$ complexes. For $ZnL^2(MeOH)$, the methyl resonances shift from 2.20 and 2.21 ppm to 2.34 and 2.35 ppm, while the hydrazinopyridine peaks shift from 6.66, 6.84, 7.56, and 7.74 ppm to 7.06, 7.12, 7.91, and 8.05 ppm. The other Zn complexes show similar shifts. To further confirm the formation of methylcarbonate, FT-IR spectra were collected on $ZnL^n(MeOH)$ solutions in 10% CD_3OD and 90% dichloromethane under Ar and CO_2. As shown for $ZnL^4(MeOH)$ (Fig. S31), the introduction of CO_2 results in a new, sharp peak at 1613 cm^{-1} and a series of broader peaks between 1629 and 1700 cm^{-1} consistent with an equilibrium mixture of bound and unbound methylcarbonate.[39] Similar spectra were obtained for the other Zn complexes (Fig. S32).

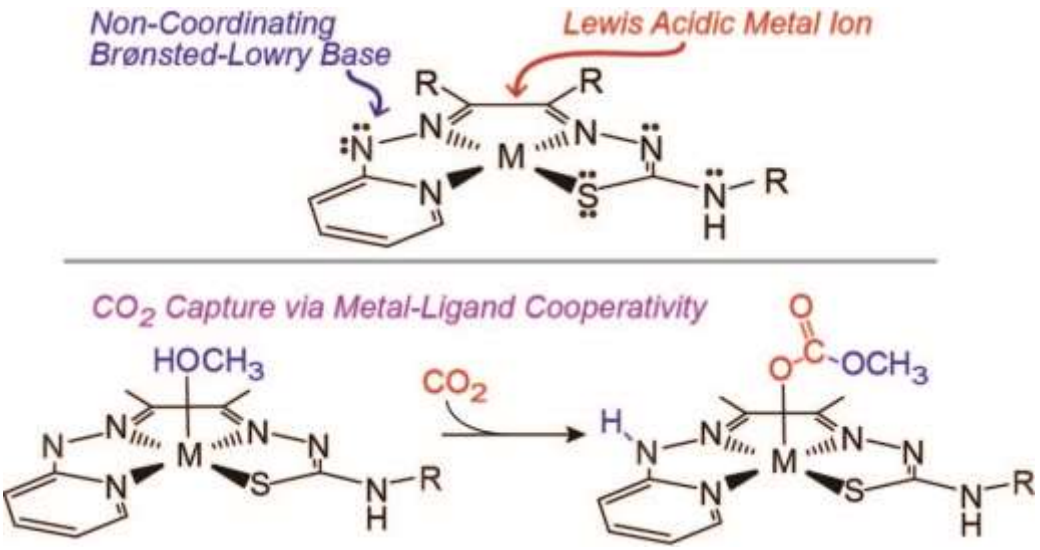

Figure 4. Metal-ligand cooperativity for CO_2 capture with ML^n(MeOH) complexes.

The equilibrium constant for CO_2 capture, K_1, associated with the reversible capture of CO_2 as a metal-bound methylcarbonate species (Scheme 1, equation 1) was determined spectrophotometrically. The color changes from orange to yellow for the Zn(II) complexes and purple to orange for CuL^1(MeOH) upon CO_2 capture associated with a change in the protonation state of the hydrazinatopyridine chromophore. As shown in Figure 5, a 0.2 mM solution of ZnL^2(MeOH) in methanol displays a prominent peak at 487 nm under Ar associated with the hydrazinatopyridine chromophore in the unprotonated state. Sparging the solution with 1 atm CO_2 results in a shift of the hydrazinatopyridine peak to 430 nm due to protonation as part of the capture process. At lower CO_2 pressures (100 – 1000 ppm), the relative intensity of the two peaks varies as a function of CO_2 concentration. Analysis of the data using Bindfit[40-42] yielded a CO_2 capture equilibrium constant (K_1) of 11,700 ± 300 for ZnL^2(MeOH). Similar measurements were conducted for the other Zn(II) and Cu(II) complexes with their associated K_1 tabulated in Table 2. Notably, ZnL^4(MeOH) has the highest equilibrium constant for CO_2 capture, K_1 = 35,000 ± 200, despite having lower basicity than the ZnL^{1-3}(MeOH) complexes. The equilibrium constant of 88

± 9 for the Cu(II) complex $CuL^1(MeOH)$ is ~400 times lower than the corresponding Zn(II) complex.

Scheme 1. Overall and stepwise CO_2 capture reactions.

Overall CO_2 Capture Reaction

$$ML^n(MeOH) + CO_2 \rightleftharpoons M(HL^n)(O_2COMe) \qquad K_1 \quad (1)$$

Protonation Reaction

$$ML^n(MeOH) + CO_2 + MeOH \rightleftharpoons [M(HL^n)(MeOH)]^+ + MeOCO_2^- \qquad K_2 \quad (2)$$

Ligand Exchange Reaction

$$[M(HL^n)(MeOH)]^+ + MeOCO_2^- \rightleftharpoons M(HL^n)(O_2COMe) + MeOH \qquad K_3 \quad (3)$$

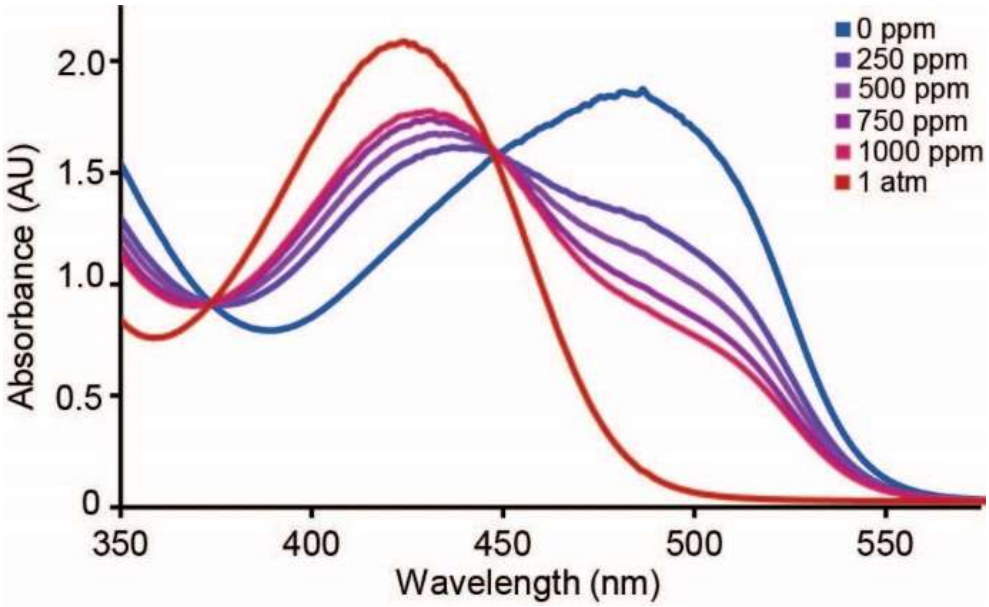

Figure 5. Spectrophotometric titration of a 0.20 mM solution of $ZnL^2(MeOH)$ in methanol under a 1 atmosphere stream of Ar/CO_2 containing 0, 250 ppm, 750 ppm, 1000 ppm, and 1 atm of CO_2.

Table 2. Equilibrium constants for $ML^n(MeOH)$ complexes with CO_2 in methanol.

Complex	K_1 CO_2 Affinity	K_2 Protonation	K_3 Ligand Exchange
$CuL^1(MeOH)$	88 ± 9	0.17 ± 0.03	520 ± 100
$ZnL^1(MeOH)$	6900 ± 180	81 ± 17	85 ± 18
$ZnL^2(MeOH)$	11,700 ± 300	105 ± 24	112 ± 26
$ZnL^3(MeOH)$	15,000 ± 400	91 ± 10	164 ± 18
$ZnL^4(MeOH)$	35,000 ± 200	21 ± 2	1670 ± 160

Thermodynamic Discussion

Metal-ligand cooperativity promotes CO_2 capture in a reaction that is dependent on the Brønsted-Lowry basicity of the hydrazinatopyridine ligand and the Lewis acidity metal ion. As shown in Scheme 1, the overall CO_2 capture reaction (equation 1) can be *conceptually represented* as the combination of a Brønsted-Lowry acid-base reaction (equation 2) and a ligand exchange reaction (equation 3). This approach provides a means to deconvolute the effect of the ligand basicity and metal acidity on the CO_2 capture reaction. It does not require the reaction mechanism necessarily proceeds via these steps. As reported for $ZnL^1(MeOH)$,[30] a mechanism involving tautomerization between $ZnL^1(MeOH)$ and $Zn(HL^1)(OMe)$, followed by CO_2 insertion is consistent with the known CO_2 reactivity of other metal-alkoxide complexes.[43-45]

The acid-base reaction in equation 2 involves a proton transfer between methylcarbonic acid (CH_3OCO_2H), formed upon dissolution of CO_2 in methanol, and the hydrazinatopyridine of $M(L^n)(MeOH)$. The dissolution of CO_2 in methanol yields small amounts of methylcarbonic acid, analogous to the formation of carbonic acid upon CO_2 dissolution in water. The effective pK_a for the acid dissociation of CO_2 in methanol to $CH_3OH_2^+$ and methylcarbonate as the conjugate base is 8.97.[46] Based on this effective pK_a and the measured pK_a values associated with the $ML^n(MeOH)$ complexes in Table 1, equilibrium constants (K_2) for the acid-base reactions were calculated. As shown in Table 2, for each of the $ML^n(MeOH)$ complexes, the overall equilibrium constant (K_1) is greater than the acid-base equilibrium constant (K_2). This clearly shows that CO_2 capture is not a simple acid-base reaction between $ML^n(MeOH)$ and methylcarbonic acid. The ratio of K_1/K_2 defines K_3, which represents the ligand exchange reaction between the weak, neutral Lewis base methanol with the much stronger, anionic Lewis base methylcarbonate and provides an indirect measure of Lewis acidity of the metal. This Lewis acidity factor increases the CO_2 capture affinity by stabilizing the conjugate base (methylcarbonate) of the acid-base reaction through coordination similar to the way HF is transformed from a weak acid to a super acid upon addition of SbF_5.

A comparison of the equilibrium constants in Table 2 reveals some interesting trends. The data for $CuL^1(MeOH)$ and $ZnL^1(MeOH)$ reveal a clear metal ion effect with a substantial *increase in CO_2 capture affinity upon substitution of Cu(II) with Zn(II)*. Within the Zn(II) series, a ligand effect is observed with the ability to *further increase CO_2 capture affinity upon variation of the ligand substituents.* For the $ML^1(MeOH)$ complexes, substitution of Cu(II) with the less Lewis acidic Zn(II) ion results in a substantial increase in the basicity of the hydrazinatopyridine nitrogen as evidenced by an increase in K_2 by a factor of ~500. However, the lower Lewis acidity of Zn(II) also decreases the affinity for methylcarbonate as demonstrated by the ~6 fold decrease in K_3.

Overall, the CO_2 capture affinity increases from 88 to 6900 upon substitution of Cu(II) with Zn(II). The CO_2 capture affinity can be further enhanced by fine tuning of the ligand. As noted above, the $ZnL^{1\text{-}3}$(MeOH) complexes have similar basicities, which leads to similar K_2 values. The observed increase in K_1 within this series results from increased Lewis acidity of the Zn(II) ion. The greatest CO_2 capture affinity is observed for ZnL^4(MeOH). The benzylamine substituent in this complex substantially increases the Lewis acidity of the Zn(II) by at least one order of magnitude relative to the other Zn complexes, as indicated by the K_3 values. However, it also slightly decreases the basicity of the non-coordinating nitrogen in the hydrazinatopyridine, by a factor of ~4, as shown in the K_2 values. The net result is a CO_2 capture affinity, K_1, for ZnL^4(MeOH) that is at least double that of the other Zn complexes. Within the other complexes, $ZnL^{1\text{-}3}$(MeOH) all have similar ligand basicities (K_2), with some variation in Lewis acidity (K_3) that is responsible for changes in CO_2 capture affinity.

Conclusion

A series of thiosemicarbazonato-hydrazinatopyridine metal complexes have been synthesized, characterized, and evaluated for their ability to capture CO_2. Although the Co(III), Ni(II), and Pd(II) complexes showed no CO_2 capture affinity, metal−ligand cooperativity facilitates CO_2 capture with the Cu(II) and Zn(II) ML^n(MeOH) complexes in methanol. The reaction involves complimentary protonation of the non-coordinated, hydrazinatopyridine nitrogen in a Brønsted-Lowry acid-base reaction and stabilization of the methylcarbonate anion via coordination to the Lewis acidic metal ion. As such, the equilibrium constant for CO_2 capture, K_1, depends on both the ligand basicity, K_2, and the metal Lewis acidity, K_3. Overall, the Zn(II) complexes bind CO_2 significantly stronger than Cu(II) due to increased ligand basicity. Variations in the Lewis acidity of the Zn(II) complexes by variation of the pendent amine on the thiosemicarbazone functional

group further enhanced CO_2 capture with the benzylamine derivative, $ZnL^4(MeOH)$, showing the best performance.

The Zn(II) complexes efficiently bind CO_2 from dilute sources such as enclosed interior spaces or air. The concentration of CO_2 within buildings typically varies from ~400 ppm (concentration in air) to 2500 ppm with 1000 ppm identified by the World Health Organization as a maximum level for indoor air quality.[47] As shown in Figure 6a, a 0.3 mM solution of $ZnL^4(MeOH)$ effectively captures 90% of the CO_2 from 400 ppm air, 86% of 1000 ppm CO_2, and 65% of 2500 ppm CO_2. The other Zn(II) complexes perform slightly less well, but all capture at least 64%, 59%, and 46% of CO_2 at 400, 1000, and 2500 ppm, respectively. The $CuL^1(MeOH)$ is significantly less effective as it binds only 2 – 3% of these dilute CO_2 streams. At higher CO_2 concentrations associated with flue gas exhaust (15% CO_2)[48] or pure CO_2 streams (1 atm) the percentage of CO_2 sequestered from these sources is very low (≤ 1%) as the metal complexes in solution are saturated with CO_2, Figure 6b. In summary, thiosemicarbazonato-hydrazinatopyridine metal complexes provide a novel route for reversible CO_2 capture from dilute sources with high CO_2 capture efficiency up to 90% from air.

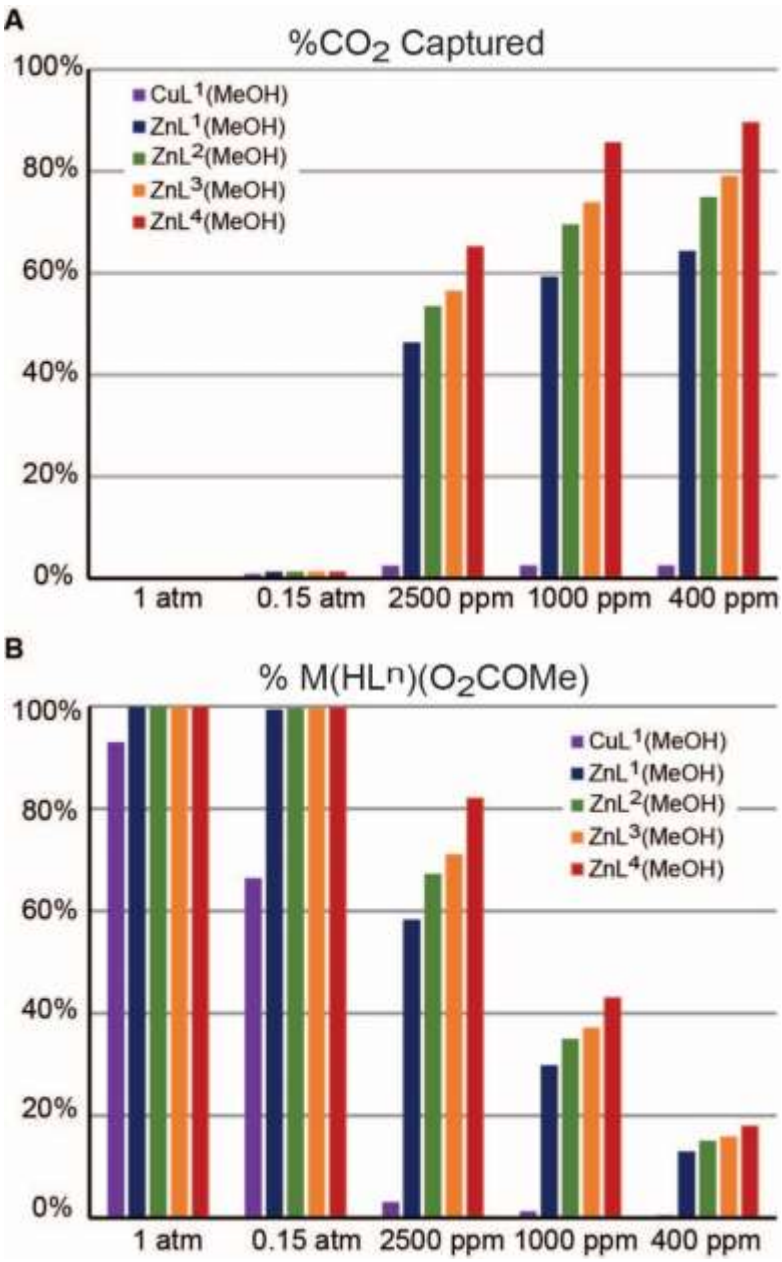

Figure 6. A) Percentage CO_2 captured by a 0.3 mM solution of $ML^n(MeOH)$ complexes at CO_2 pressures from 400 ppm to 1 atm. B) Percentage of $M(HL^n)(O_2COMe)$ complexes in a 0.3 mM solution of $ML^n(MeOH)$ from 400 ppm to 1 atm of CO_2.

ASSOCIATED CONTENT

Supporting Information

The following files are available free of charge: crystallographic data and refinement parameters; NMR and UV-visible spectra (PDF). CCDC 2214614−2214616 contain the supplementary crystallographic data for this paper. These data can be obtained free of charge via www.ccdc.cam.ac.uk/data_request/cif, or by emailing data_request@ccdc.cam.ac.uk, or by contacting The Cambridge Crystallographic Data Centre, 12 Union Road, Cambridge CB2 1EZ, UK; fax: +44 1223 336033.

AUTHOR INFORMATION

Corresponding Author

Craig Grapperhaus, email: craig.grapperhaus@louisville.edu, ORCID 0000-0003-4889-2645

Robert Buchanan email: robert.buchanan@louisville.edu, ORCID 0000-0001-8653-5388

Other Authors

Christine A. Phipps, ORCID 0000-0003-4924-7488

Dillon T. Hofsommer, ORCID 0000-0001-8638-2465

Calian D. Zirilli, ORCID 0000-0002-5784-5595

Bailee G. Duff, ORCID 0000-0003-2725-9832

Mark S. Mashuta, ORCID 0000-0002-2724-7252

Author Contributions

C.D.Z. and B.G.D. performed ligand and complex syntheses and assisted with the collection of spectroscopic data. D.T.H. synthesized and characterized $[CoL^1(PPh_3)]BF_4$. M.S.M. performed all X-ray crystallography. C.A.P. performed all other experiments in the manuscript. D.T.H. and C.A.P. wrote the manuscript in tandem. D.T.H, R.M.B., and C.A.G. conceived the project, supervised experimental studies, and contributed to writing the manuscript. All authors have approved the final version of the manuscript.

Funding Sources

This research was supported by the National Science Foundation CHE-1955268 (CAG) and CHE-1800245 (RMB).

Notes

The authors declare no competing financial interests.

References

1. House, K. Z.; Baclig, A. C.; Ranjan, M.; Nierop, E. A. v.; Wilcox, J.; Herzog, H. J. Economic and energetic analysis of capturing CO_2 from ambient air. *Proc. Natl. Acad. Sci. U. S. A.* **2011**, *108* (51), 20428-20433. DOI: 10.1073/pnas.1012253108.
2. Rendell, D. J.; Clarke, M.; Evans, M. The Effect of Environmental Conditions on The Absorption of Carbon Dioxide Using Soda Lime. SAE Technical Paper 2003-01-2644, 2003 DOI: 10.4271/2003-01-2644.
3. Boyda, R. B.; Miller, C. W.; Schwartz, M. R. Integrated Air Revitalization System for Space Station. *SAE Transactions* **1986**, *95*, 207 -219.
4. Fasihi, M.; Efimova, O.; Breyer, C. Techno-economic assessment of CO_2 direct air capture plants. *J. Clean. Prod.* **2019**, *224*, 957-980. DOI: 10.1016/j.jclepro.2019.03.086.
5. Sanz-Pérez, E. S.; Murdock, C. R.; Didas, S. A.; Jones, C. W. Direct Capture of CO2 from Ambient Air. *Chem. Rev.* **2016**, *116* (19), 11840-11876. DOI: 10.1021/acs.chemrev.6b00173.
6. Wang, Y.-B.; Sun, D.-S.; Zhou, H.; Zhang, W.-Z.; Lu, X.-B. CO_2, COS and CS_2 adducts of N-heterocyclic olefins and their application as organocatalysts for carbon dioxide fixation. *Green Chemistry* **2015**, *17* (7), 4009-4015, 10.1039/C5GC00948K. DOI: 10.1039/C5GC00948K.

7. Lee , C.-H.; Huang , H.-Y.; Lee, J.-J.; Huang, C.-Y.; Kao, Y.-C.; Lee, G.-H.; Peng , S.-M.; Jiang, J.-C.; Chao, I.; Lu, K.-L. Amide-CO_2 Interaction Induced Gate-Opening Behavior for CO_2 Adsorption in 2-Fold Interpenetrating Framework. *ChemistrySelect* **2016**, *1* (11), 2923-2929. DOI: 10.1002/slct.201600345.
8. Chen, C.; Li, X.; Zou, W.; Wan, H.; Dong, L.; Guan, G. Structural modulation of UiO-66-NH_2 metal-organic framework via interligands cross-linking: Cooperative effects of pore diameter and amide group on selective CO_2 separation. *Appl. Surf. Sci.* **2021**, *553*, 149547. DOI: 10.1016/j.apsusc.2021.149547.
9. Park, J.; Li, J.-R.; Chen, Y.-P.; Yu, J.; Yakovenko, A. A.; Wang, Z. U.; Sun, L.-B.; Balbuena, P. B.; Zhou, H.-C. A versatile metal–organic framework for carbon dioxide capture and cooperative catalysis. *Chem. Commun.* **2012**, *48* (80), 9995-9997. DOI: 10.1039/C2CC34622B.
10. Ma, L.; Wang, X.; Deng, D.; Luo, F.; Ji, B.; Zhang, J. Five porous zinc(II) coordination polymers functionalized with amide groups: cooperative and size-selective catalysis. *J. Mater. Chem. A* **2015**, *3* (40), 20210-20217. DOI: 10.1039/C5TA06248A.
11. Smith, A. L.; Hardcastle, K. I.; Soper, J. D. Redox-active ligand-mediated oxidative addition and reductive elimination at square planar cobalt(III): Multielectron reactions for cross-coupling. *J. Am. Chem. Soc.* **2010**, *132* (41), 14358-14360. DOI: 10.1021/ja106212w.
12. van der Meer, M.; Rechkemmer, Y.; Peremykin, I.; Hohloch, S.; van Slageren, J.; Sarkar, B. (Electro)catalytic C–C bond formation reaction with a redox-active cobalt complex. *Chem. Commun.* **2014**, *50* (76), 11104-11106. DOI: 10.1039/C4CC03309D.
13. Haneline, M. R.; Heyduk, A. F. C−C Bond-Forming Reductive Elimination from a Zirconium(IV) Redox-Active Ligand Complex. *J. Am. Chem. Soc.* **2006**, *128* (26), 8410-8411. DOI: 10.1021/ja061107a.
14. Tennyson, A. G.; Lynch, V. M.; Bielawski, C. W. Arrested Catalysis: Controlling Kumada Coupling Activity via a Redox-Active N-Heterocyclic Carbene. *J. Am. Chem. Soc.* **2010**, *132* (27), 9420-9429. DOI: 10.1021/ja102686u.
15. Guin, A. K.; Mondal, R.; Chakraborty, G.; Pal, S.; Paul, N. D. Ruthenium-Catalyzed Dehydrogenative Functionalization of Alcohols to Pyrroles: A Comparison between Metal–Ligand Cooperative and Non-cooperative Approaches. *J. Org. Chem.* **2022**, *87* (11), 7106-7123. DOI: 10.1021/acs.joc.2c00311.
16. Sikari, R.; Sinha, S.; Chakraborty, G.; Das, S.; van Leest, N. P.; Paul, N. D. C−N Cross-Coupling Reactions Under Mild Conditions Using Singlet Di-Radical Nickel(II)-Complexes as Catalyst: N-Arylation and Quinazoline Synthesis. *Adv. Synth. Catal.* **2019**, *361* (18), 4342-4353. DOI: 10.1002/adsc.201900545.
17. Russell, S. K.; Lobkovsky, E.; Chirik, P. J. Iron-Catalyzed Intermolecular [2π + 2π] Cycloaddition. *J. Am. Chem. Soc.* **2011**, *133* (23), 8858-8861. DOI: 10.1021/ja202992p (acccessed 2011/11/21).
18. Sylvester, K. T.; Chirik, P. J. Iron-catalyzed, hydrogen-mediated reductive cyclization of 1,6-enynes and diynes: Evidence for bis(imino)pyridine ligand participation. *J. Am. Chem. Soc.* **2009**, *131* (25), 8772-8774. DOI: 10.1021/ja902478p.
19. Brunel, P.; Monot, J.; Kefalidis, C. E.; Maron, L.; Martin-Vaca, B.; Bourissou, D. Valorization of CO_2: Preparation of 2-Oxazolidinones by Metal–Ligand Cooperative Catalysis with SCS Indenediide Pd Complexes. *ACS Catal.* **2017**, *7* (4), 2652-2660. DOI: 10.1021/acscatal.7b00209.
20. Zubar, V.; Lebedev, Y.; Azofra, L. M.; Cavallo, L.; El-Sepelgy, O.; Rueping, M. Hydrogenation of CO_2-Derived Carbonates and Polycarbonates to Methanol and Diols by Metal–

Ligand Cooperative Manganese Catalysis. *Angew. Chem. Int. Ed.* **2018**, *57* (41), 13439-13443. DOI: 10.1002/anie.201805630.
21. Chen, Y.; Li, H.; Zhao, W.; Zhang, W.; Li, J.; Li, W.; Zheng, X.; Yan, W.; Zhang, W.; Zhu, J.; Si, R.; Zeng, J. Optimizing reaction paths for methanol synthesis from CO_2 hydrogenation via metal-ligand cooperativity. *Nat. Commun.* **2019**, *10* (1), 1885. DOI: 10.1038/s41467-019-09918-z.
22. Mathis, C. L.; Geary, J.; Ardon, Y.; Reese, M. S.; Philliber, M. A.; VanderLinden, R. T.; Saouma, C. T. Thermodynamic Analysis of Metal–Ligand Cooperativity of PNP Ru Complexes: Implications for CO_2 Hydrogenation to Methanol and Catalyst Inhibition. *J. Am. Chem. Soc.* **2019**, *141* (36), 14317-14328. DOI: 10.1021/jacs.9b06760.
23. Elsby, M. R.; Baker, R. T. Strategies and mechanisms of metal–ligand cooperativity in first-row transition metal complex catalysts. *Chem. Soc. Rev.* **2020**, *49* (24), 8933-8987. DOI: 10.1039/D0CS00509F.
24. Rauch, M.; Kar, S.; Kumar, A.; Avram, L.; Shimon, L. J. W.; Milstein, D. Metal–Ligand Cooperation Facilitates Bond Activation and Catalytic Hydrogenation with Zinc Pincer Complexes. *J. Am. Chem. Soc.* **2020**, *142* (34), 14513-14521. DOI: 10.1021/jacs.0c05500.
25. Vogt, M.; Gargir, M.; Iron, M. A.; Diskin-Posner, Y.; Ben-David, Y.; Milstein, D. A New Mode of Activation of CO_2 by Metal–Ligand Cooperation with Reversible C-C and M-O Bond Formation at Ambient Temperature. *Chem. Eur. J.* **2012**, *18* (30), 9194-9197. DOI: 10.1002/chem.201201730.
26. McKinnon, M.; Ngo, K. T.; Sobottka, S.; Sarkar, B.; Ertem, M. Z.; Grills, D. C.; Rochford, J. Synergistic Metal–Ligand Redox Cooperativity for Electrocatalytic CO_2 Reduction Promoted by a Ligand-Based Redox Couple in Mn and Re Tricarbonyl Complexes. *Organometallics* **2019**, *38* (6), 1317-1329. DOI: 10.1021/acs.organomet.8b00584.
27. Filonenko, G. A.; Conley, M. P.; Copéret, C.; Lutz, M.; Hensen, E. J. M.; Pidko, E. A. The impact of Metal–Ligand Cooperation in Hydrogenation of Carbon Dioxide Catalyzed by Ruthenium PNP Pincer. *ACS Catal.* **2013**, *3* (11), 2522-2526. DOI: 10.1021/cs4006869.
28. Sieh, D.; Lacy, D. C.; Peters, J. C.; Kubiak, C. P. Reduction of CO_2 by Pyridine Monoimine Molybdenum Carbonyl Complexes: Cooperative Metal–Ligand Binding of CO_2. *Chem. Eur. J.* **2015**, *21* (23), 8497-8503. DOI: 10.1002/chem.201500463.
29. Derrick, J. S.; Loipersberger, M.; Chatterjee, R.; Iovan, D. A.; Smith, P. T.; Chakarawet, K.; Yano, J.; Long, J. R.; Head-Gordon, M.; Chang, C. J. Metal–Ligand Cooperativity via Exchange Coupling Promotes Iron-Catalyzed Electrochemical CO_2 Reduction at Low Overpotentials. *J. Am. Chem. Soc.* **2020**, *142* (48), 20489-20501. DOI: 10.1021/jacs.0c10664.
30. Cronin, S. P.; Strain, J. M.; Mashuta, M. S.; Spurgeon, J. M.; Buchanan, R. M.; Grapperhaus, C. A. Exploiting Metal–Ligand Cooperativity to Sequester, Activate, and Reduce Atmospheric Carbon Dioxide with a Neutral Zinc Complex. *Inorg. Chem.* **2020**, *59* (7), 4835-4841. DOI: 10.1021/acs.inorgchem.0c00121.
31. Cowley, A. R.; Dilworth, J. R.; Donnelly, P. S.; White, J. M. Copper Complexes of Thiosemicarbazone−Pyridylhydrazine (THYNIC) Hybrid Ligands: A New Versatile Potential Bifunctional Chelator for Copper Radiopharmaceuticals. *Inorg. Chem.* **2006**, *45* (2), 496-498. DOI: 10.1021/ic0514492.
32. Calatayud, D. G.; Lopez-Torres, E.; Dilworth, J. R.; Antonia Mendiola, M. Complexes of group 12 metals containing a hybrid thiosemicarbazone-pyridylhydrazone ligand. *Inorg. Chim. Acta* **2012**, *381*, 150-161. DOI: 10.1016/j.ica.2011.10.023.

33. Phipps, C. A.; Hofsommer, D. T.; Toda, M. J.; Nkurunziza, F.; Shah, B.; Spurgeon, J. M.; Kozlowski, P. M.; Buchanan, R. M.; Grapperhaus, C. A. Ligand-Centered Hydrogen Evolution with Ni(II) and Pd(II)DMTH. *Inorg. Chem.* **2022**, *61* (25), 9792-9800. DOI: 10.1021/acs.inorgchem.2c01326.
34. Huang, H.; Chen, Q.; Ku, X.; Meng, L.; Lin, L.; Wang, X.; Zhu, C.; Wang, Y.; Chen, Z.; Li, M.; Jiang, H.; Chen, K.; Ding, J.; Liu, H. A Series of α-Heterocyclic Carboxaldehyde Thiosemicarbazones Inhibit Topoisomerase IIα Catalytic Activity. *J. Med. Chem.* **2010**, *53* (8), 3048-3064. DOI: 10.1021/jm9014394.
35. Chiswell, B.; Lions, F.; Tomlinson, M. L. Tridentate Chelate Compounds. IV. Metal Complexes from α-Diketone Mono-α-pyridylhydrazone Type Ligands. *Inorg. Chem.* **1964**, *3* (4), 492-499. DOI: 10.1021/ic50014a007.
36. *CrysAlis PRO (CCD and RED), V 1.171.40.67a*; Rigaku OD 2019.
37. *SCALE3 ABSPACK included in CrysAlis PRO RED, V. 1.171.40.67a*.
38. Sheldrick, G. M. A short history of SHELX. *Acta Crystallogr A* **2008**, *64* (1), 112-122. DOI: 10.1107/S0108767307043930.
39. Hong, S. Y.; Cheon, Y.; Shin, S. H.; Lee, H.; Cheong, M.; Kim, H. S. Carboxylate-Assisted Formation of Alkylcarbonate Species from CO_2 and Tetramethylammonium Salts with a β-Amino Acid Anion. *ChemSusChem* **2013**, *6* (5), 890-897. DOI: 10.1002/cssc.201200971.
40. Brynn Hibbert, D.; Thordarson, P. The death of the Job plot, transparency, open science and online tools, uncertainty estimation methods and other developments in supramolecular chemistry data analysis. *Chem. Commun.* **2016**, *52* (87), 12792-12805. DOI: 10.1039/C6CC03888C.
41. Thordarson, P. Determining association constants from titration experiments in supramolecular chemistry. *Chem. Soc. Rev.* **2011**, *40* (3), 1305-1323. DOI: 10.1039/C0CS00062K.
42. Bindfit. http://supramolecular.org/.
43. Arikawa, Y.; Nakamura, T.; Ogushi, S.; Eguchi, K.; Umakoshi, K. Fixation of atmospheric carbon dioxide by ruthenium complexes bearing an NHC-based pincer ligand: formation of a methylcarbonato complex and its methylation. *Dalton Trans.* **2015**, *44* (12), 5303-5305. DOI: 10.1039/C5DT00476D.
44. Mandal, S. K.; Ho, D. M.; Orchin, M. Reaction of electrophiles with manganese(I) and rhenium(I) alkoxide complexes: reversible absorption of atmospheric carbon dioxide. *Organometallics* **1993**, *12* (5), 1714-1719. DOI: 10.1021/om00029a032.
45. Kato, M.; Ito, T. Facile carbon dioxide uptake by zinc(II)-tetraazacycloalkane complexes. 2. X-ray structural studies of (.mu.-monomethyl carbonato)(1,4,8,11-tetraazacyclotetradecane)zinc(II) perchlorate, bis(.mu.-monomethyl carbonato)tris[(1,4,8,12-tetraazacyclopentadecane)zinc(II)] perchlorate, and (monomethyl carbonato)(1,4,8,11-tetramethyl-1,4,8,11-tetraazacyclotetradecane)zinc(II) perchlorate. *Inorg. Chem.* **1985**, *24* (4), 509-514. DOI: 10.1021/ic00198a016.
46. Gohres, J. L.; Marin, A. T.; Lu, J.; Liotta, C. L.; Eckert, C. A. Spectroscopic investigation of alkylcarbonic acid formation and dissociation in CO_2 expanded alcohols. *Ind. Eng. Chem. Res.* **2009**, *48* (3), 1302-1306.
47. Ma, N.; Aviv, D.; Guo, H.; Braham, W. W. Measuring the right factors: A review of variables and models for thermal comfort and indoor air quality. *Renewable and Sustainable Energy Rev.* **2021**, *135*, 110436. DOI: 10.1016/j.rser.2020.110436.

48. Gautam, M.; Hofsommer, D. T.; Uttarwar, S. S.; Theaker, N.; Paxton, W. F.; Grapperhaus, C. A.; Spurgeon, J. M. The effect of flue gas contaminants on electrochemical reduction of CO_2 to methyl formate in a dual methanol/water electrolysis system. *Chem Catalysis* **2022**, *2* (9), 2364-2378. DOI: 10.1016/j.checat.2022.08.001.

TOC Image and Synopsis

Thiosemicarbazonato-hydrazinatopyridine metal complexes reversibly capture CO_2 as metal bound methylcarbonate. Substitution of Cu(II) with Zn(II) improves CO_2 capture affinity by modulating ligand basicity while variation of the thiosemicarbazone ligand enhances CO_2 affinity by tuning the metal ion Lewis acidity. Overall, the Zn(II) complexes effectively capture CO_2 from dilute sources with up to 90%, 86%, and 65% CO_2 capture efficiency from 400 ppm, 1000 ppm, and 2500 ppm CO_2 streams.